

Investigations of Direct Containment Heating (DCH) in European Reactors: Database of Integral Tests and Progress in Modeling

C. Spengler¹, L. Meyer², R. Meignen³

CONTRACT SARNET FI60-CT-2004-509065

- 1) Gesellschaft für Anlagen- und Reaktorsicherheit *GRS*, Cologne (DE)
- 2) Forschungszentrum Karlsruhe *FZK*, Karlsruhe (DE)
- 3) Institut de Radioprotection et de Sûreté Nucléaire *IRSN*, Paris (FR)

Summary

The DISCO test facility at Forschungszentrum Karlsruhe (FZK) has been used to perform experiments to investigate direct containment heating (DCH) effects during a severe accident in European nuclear power plants, comprising the EPR, the French 1300 MWe plant P'4, the VVER-1000 and the German Konvoi plant. A high-temperature iron-alumina melt is ejected by steam into scaled models of the respective reactor cavities and the containment vessel. Both heat transfer from dispersed melt and combustion of hydrogen lead to containment pressurization. The main experimental findings are presented and critical parameters are identified.

In the framework of SARNET part of this experimental data base is subject for a common interpretation work performed by the participating organizations, including application and assessment of the DCH in MAAP, ASTEC/RUPUICUV, COCOSYS and CONTAIN. Even the more mechanistic approaches in the models require the use and adoption of empirical parameters which are specific to the layout of the plant and which have significant impact on the calculations. Based on the calculations the models are compared and their potential for predictions is assessed. Supporting analyses are performed with the multi-fluid code MC3D for a deepened understanding of the key processes of melt fragmentation and dispersal.

A. INTRODUCTION

In case of a core meltdown accident in a PWR, liquid corium containing metals and oxides may relocate into the lower head of the reactor vessel. If the lower head fails in this condition, with an in-vessel pressure higher than the containment pressure, the molten corium will be forcefully ejected into the reactor pit, finely fragmented and eventually transported outside the reactor pit. The efficient heat transfer from the melt particles to the gas, together with combustion of hydrogen previously released into the reactor building and produced during melt dispersion, will heat-up and pressurize the containment atmosphere. These processes, referred to as Direct Containment Heating (DCH), may endanger the integrity of the containment.

The safety philosophy applied to all plants worldwide is to prevent high pressure core melt situations by depressurization of the primary system below a level which would be effective in limiting debris dispersal mainly to the reactor pit or adjacent small reactor rooms. This level, sometimes called the DCH cut-off pressure, depends on reactor cavity design and lies between 1.0 and 2.5 MPa, but can be as low as 0.5 MPa for certain plant geometries. If the occurrence of DCH is related with the primary circuit pressure at vessel failure, its consequences depend also on the breach characteristics, on the amount and characteristics of the

molten mass and on the layout of the reactor pit and reactor building. Therefore, the evaluation of DCH consequences must be plant dependent.

B. EXPERIMENTAL DATA BASE

A large amount of work has been done in the '80s and '90s, mainly in the USA, to investigate the melt dispersal/DCH-phenomena for cavity designs with large instrument tunnels leading into sub-compartments (Westinghouse plants). Only a few experiments had been done with an annular cavity design, where the only or main large pathway out of the cavity is along the annular gap between the RPV and the cavity wall with direct access to the containment dome [1]. The state of the art as of 1996 was given by Pilch et al. [2].

A key role for the increase of the containment pressure plays the fraction of hot debris particles dispersed into large reactor rooms, such as the upper containment. A number of correlations were developed in the past to relate the debris dispersal to reactor vessel failure pressure via gas velocity and to ratios of flow areas out of the pit. The results have shown that these correlations developed mainly for Westinghouse geometry are not applicable for plant geometries with annular cavity design.

To generate data on melt dispersion applicable to European reactor plants a series of experiments with cold model fluids was performed in the DISCO-C facility at Forschungszentrum Karlsruhe (FZK), which are limited to the fluid dynamic processes [3,4,5]. While these experiments serve well to validate models in codes, correlations for melt dispersal derived from these data should be applied with caution to the prototypic case. The thermal and chemical effects in the cavity during steam blowdown can alter the behavior of the melt particles considerably. Additionally, the effect of the different physical properties of the materials used must be well known to apply such correlations to steam and corium melts.

More prototypic tests were performed in the DISCO-H facility employing an iron-alumina melt as corium simulant, steam in the reactor pressure vessel and a prototypic atmosphere in the containment [6-10]. The analysis of these experiments showed that the combustion of hydrogen produced by oxidation as well as the hydrogen initially present in the containment can be the dominant phenomenon for the containment pressurization. This combustion is very complex because it combines the characteristics of a diffusion flame (jet of hydrogen) with the characteristics of a premixed flame (combustion of initially present hydrogen). To address this issue, a series of complementary separate effects tests in the DISCO-H facility was conducted, in a basic geometry and in the geometries of the EPR and the French P'4 cavity [11, 12]. In these tests hydrogen or a mixture of steam and hydrogen is blown out of the pressure vessel into the cavity and beyond into an atmosphere of air and steam with various contents of hydrogen. Ignition devices were placed in different locations in the reactor containment to simulate the ignition by hot debris. The modeling work with dedicated combustion codes is ongoing.

In this paper we will concentrate on the results of the integral experiments with iron-alumina melt and steam.

B.1. Design Characteristics of European PWRs

Most European PWRs have an annular cavity design, with a flow path around the main cooling lines into pump and steam generator rooms, and in some cases with a direct flow path from the reactor pit into the upper dome of the containment. Since ten years these reactor geometries are being investigated experimentally and analytically at Forschungszentrum

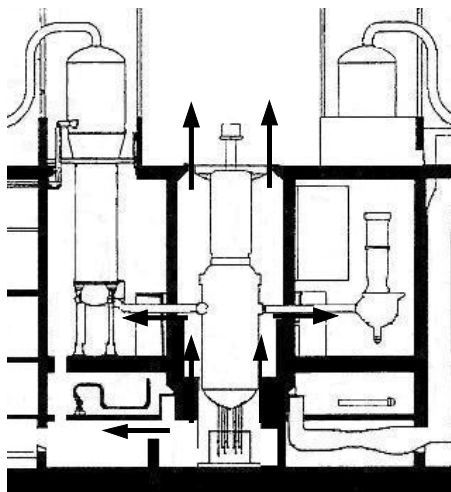


Fig. 1. Configuration of the French P'4 plant

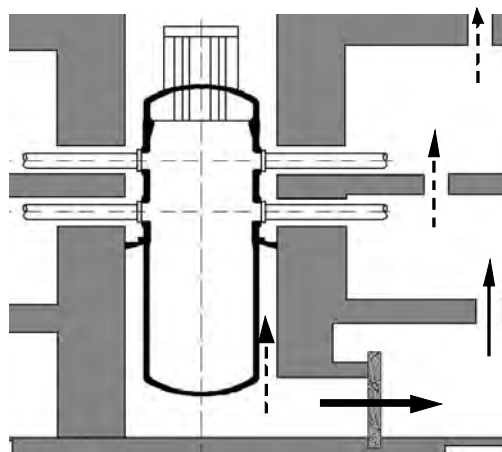


Fig. 2. Configuration of a VVER-1000 plant

Karlsruhe (FZK), comprising the EPR, [3,4,6,7,8] the French 1300 MWe plant P'4, [5] the VVER 1000/320 [9] and currently the German Konvoi plant [10].

The cavity of the *French 1300 MWe P'4* reactor (Fig. 1) has a niche and an exit at the bottom of the pit (1.6 m²) leading into a small room with relatively small connections to other rooms. The other path along which the corium may leave the lower part of the reactor pit is the annular space between reactor pit and vessel (2.9 m²). This leads vertically quasi-straight through obstacles into the upper containment (3.0 m²), and as a second path, through the horizontal annular spaces coaxial to the hot and cold legs into the pump and steam generator rooms (10 m²), which are open to the containment dome. The distance between the lower head of the pressure vessel and the pit floor is quite large.

In the *VVER-1000/320 (Kozloduy NPP)* reactor the distance between the lower head and the pit floor is smaller and the lower part of reactor pit is practically closed, except for venting lines at the pit bottom and wall (not shown in Fig. 2). The flow cross section through the vessel support structure is negligible (0.35 m²). Similar to the P'4 reactor, the pit has an access hatch (5.4 m²), but this is closed by a steel door, which can withstand a pressure of 5 bar. The room behind is connected to the containment dome via other rooms without direct path to the dome.

The reactor cavity of the *EPR* (Fig. 3) is similar to the cavity of a Combustion Engineering plant; it is narrow with a small distance between pressure vessel lower head and pit floor, and the only relevant flow path out of the lower pit is along the annular gap between the reactor pressure vessel (RPV) and the cavity wall (7.0 m² without insulation) with some constriction at the vessel support girder. Different to a Combustion Engineering plant, the direct path straight up to the containment dome is blocked, and the only exit is through the horizontal annular spaces coaxial to the main cooling lines into the pump and steam generator rooms (10 m², without insulation), which are open to the containment dome.

The reactor pit of the German *Konvoi* plant (Fig. 4) is similar to the EPR pit, except for the biological shield, which does not have a significant effect in respect to melt dispersion out of the pit. Eight pressure venting flaps behind the biological shield can be assumed to be open during the accident and water would be present blocking the free flow. According to expert judgment this flow path can be assumed to be closed for the DCH scenario. However, it is not clear if the water column can be driven out during the DCH time scale. The inspection door near the pit bottom can be assumed to stay closed. Different from the EPR the vessel support structure is located above the main cooling lines, and it blocks any direct flow path vertically into the refueling room above the pressure vessel. It is closed during normal operation by

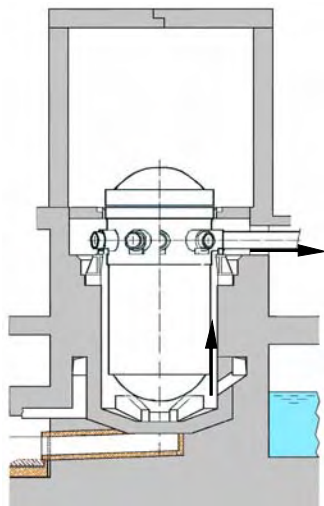


Fig. 3. Configuration of the EPR plant

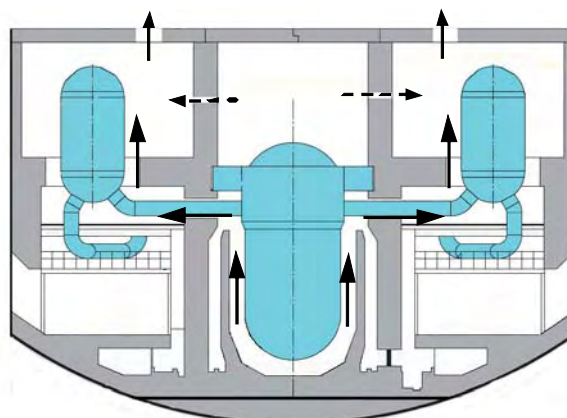


Fig. 4. Configuration of the German Konvoi plant

sealing plates, which may break away when the overpressure in the pit is above 2 bar. In that case melt transport into the relatively small refueling room would be possible through a labyrinth with an estimated flow cross section between 0.8 and 2.5 m². This room is connected to the steam generator rooms by two pressure venting flaps with small cross sections, and is covered with concrete slabs, which stay in place up to an overpressure of 0.8 bar. The only flow path open without major restriction is that along the main cooling lines into steam generator rooms (between 2.0 and 3.3 m², depending on existence of insulation). The steam generator rooms and connected rooms are closed

against the upper containment dome with approximately 240 rectangular burst diaphragms with a total cross section of 200 m². Since they would fail at a differential pressure of 48 mbar, this cross section can be assumed as an open flow path.

B.2. Experiment description

B.2.1. Components of the DISCO facility

The main components of the DISCO facility are shown in Fig. 5. The model of the containment pressure vessel has a height of 5.80 m and a total volume of 14 m³. The volumes of the reactor cooling system (RCS) and the reactor pressure vessel (RPV) are modeled by a vertical pipe. The RPV model, mounted at the lower end of the pipe, serves as crucible for the generation of melt by a thermite reaction between iron oxide and aluminum. The total volume of the RCS/RPV vessel is 0.08 m³. The breach in the lower head is modeled by a graphite annulus at the bottom, which is closed with a brass plate. This plate melts when the thermite reaction reaches the bottom.

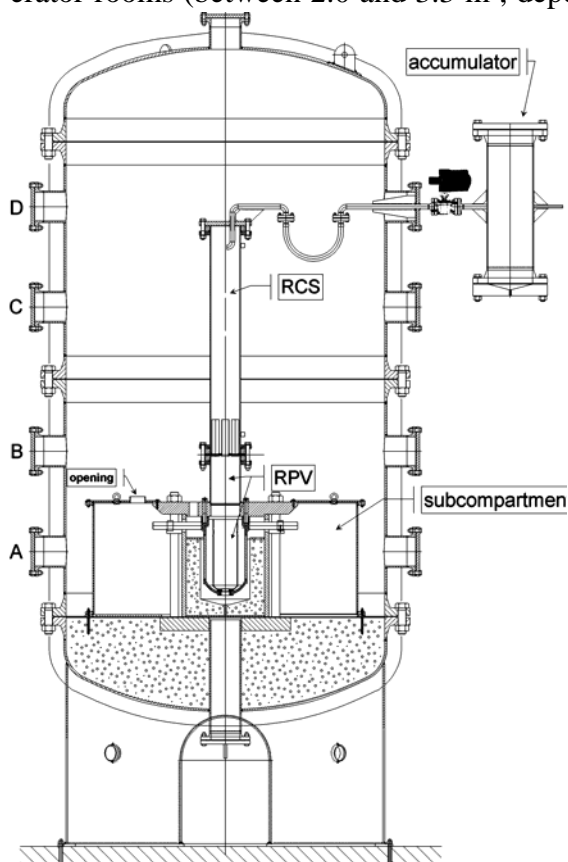


Fig. 5. Scheme of the DISCO-H facility with the model of the EPR cavity

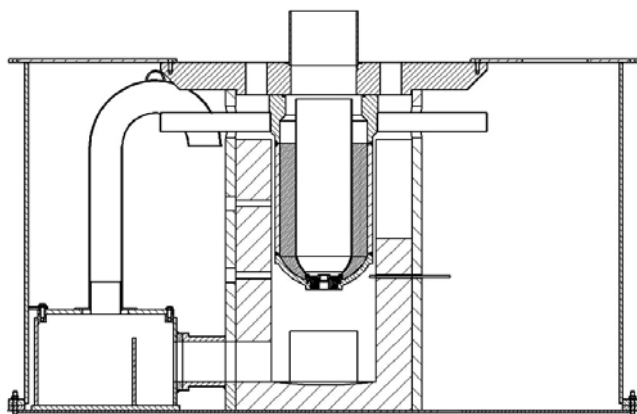


Fig. 6. Model of the P'4 cavity and compartments

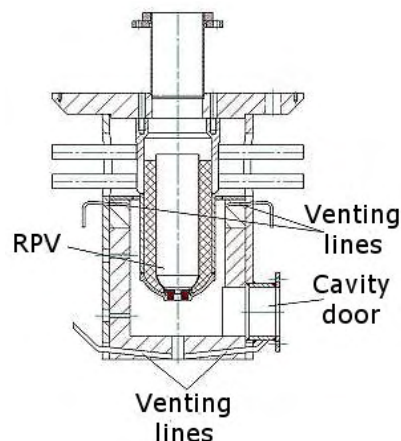


Fig. 7. Model of the VVER-1000 cavity

The reactor pit is made of concrete and is installed inside a strong steel vessel. The main cooling lines are modeled by eight horizontal steel cylinders with a scaled annular space around each of them, modeling the flow path leading into the equipment rooms. For the geometry of the P'4 plant an opening at the bottom of the pit is connected to the pit bottom access room, which has a venting line leading into the compartment (Fig. 6). A similar opening exists in the VVER-1000 pit, but this is closed by a steel plate which gives way at a differential pressure of 4 bar (Fig.7).

The equipment rooms are modeled as one annular compartment around the cavity. In case of the Konvoi reactor, a second, smaller annular subcompartment on top of the cavity models the refueling room (Fig. 8). Eight openings located in the top plate of the cavity lead into this compartment, or directly into the containment dome, depending on the reactor investigated. These openings can be closed for modeling cases, where this flow path is not available (so-called closed cavity).

A steam accumulator is connected by a 25 mm diameter pipe with an electro-pneumatically actuated valve to the containment pressure vessel.

B.2.2. Melt mass composition and scaling considerations

In the DISCO facility the outer diameter of the RPV model (298.5 mm) was kept unchanged in all experiments. The scaling of the experiment is defined by the ratio between the diameter of the respective RPV and the DISCO model. Consequently, the linear scale varies

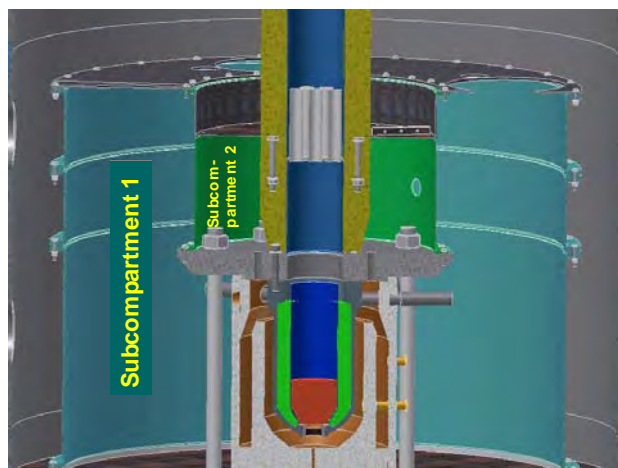


Fig. 8. Model of the Konvoi cavity and compartments

Table 1. Melt composition

	Mass (kg)	Volume (cm ³)	Moles (g mol)
Fe	5.64	887	101
Al	0.11	59	4
Al ₂ O ₃	4.88	1734	48
Total	10.64	2680	153

for the different reactor plants according to the diameter of the RPV (EPR: 1:18.0, Konvoi: 18.5, P'4: 16.4, VVER-1000: 15.2). The flow cross sections, scaled to the square of the linear scale, and the volumes of the compartments, scaled to the cube, were modeled as close as possible to the respective prototype (s. Table 2). The total volume of the containment vessel was kept constant (total freeboard volume including compartment is 13.88 m³) and therefore this scaling was not accurate in all cases. That has to be taken into account when experimental results are transferred to reactor scale.

Geometric scaling of the melt mass for the experiment is not strictly applicable because of material property differences between corium and iron-alumina melt. The mass of melt used in experiments should be selected so that it would have the same potential for pressurization as corium. Important for the similarity of thermal and chemical processes is the energy content of the melt. The chemical energy is that by the exothermic steam-metal reaction coupled with hydrogen production. The combined thermal and chemical energy is approximately 1.5 MJ/kg for a typical corium and 2.8 MJ/kg for the model melt. Thus the scaling of melt mass is difficult. The melt employed in all DISCO experiments consisted of 5.6 kg of iron, 4.9 kg of aluminum oxide and 0.1 kg aluminum (Table 1). For a linear scale 1:18, the scaling of 10.6 kg experimental melt gives: a mass of 62 tons, a volume of 16 m³, and an energy content of 175000 MJ. The volume of 16 m³ corium would have a mass of 128 tons and a total energy of 188000 MJ. Thus, the volume and energy content is scaled relatively correct (less than 10% discrepancy), while the volume - mass scaling is off by a factor of 2. This has to be taken into account when extrapolating experimental results to reactor scale, additional to the effect of different physical properties of corium and experimental melts.

The initial pressure can be scaled 1:1, and the duration of the blow down is scaled as the length scale. Then, the gas velocity and the droplet size are mainly functions of the properties of the model fluids used.

B.2.3. Experimental procedure

The containment vessel is closed at atmospheric pressure and room temperature. In most experiments a containment atmosphere was aimed at, as it can be expected during a core melt accident, with steam and a certain hydrogen content. For a period of up to 8 hours steam is filled into the containment vessel additional to the air atmosphere until the pressure reaches 0.2 MPa and the gas temperature is close to 100 °C, while the condensate is frequently drained. At the end of heat-up a metered amount of hydrogen gas (3 - 6 mol-%) is added through pipes leading into the subcompartment and the upper dome. Two fans are running until the blowdown is started, to ensure a well mixed atmosphere. A gas sample is taken just before the start of the experiment. The accumulator is pressurized with steam to around twice the planned initial blow down pressure. The model of the RPV contains the aluminum-iron oxide thermite. The experiment is started by igniting the thermite electro-chemically at the upper surface of the compacted thermite powder. When the pressure raise in the RPV-RCS vessel verifies that the thermite reaction has started, the valve in the line connected to the steam accumulator is opened and steam enters the RCS vessel, which is preheated to the saturation temperature of the planned burst pressure. The pressure balance in both vessels is reached quickly and the valve is automatically closed again. About 3 to 6 seconds after ignition the brass plug at the bottom of the RPV vessel is melted by the 2400 K hot iron-alumina mixture. That initiates the melt ejection. The melt is driven out of the breach by the steam and is dispersed into the cavity and beyond. 10 seconds after blowdown the fans are started again and five minutes thereafter post test gas samples are taken.

B.2.4. Instrumentation and measurements

Standard test results are: pressure and temperature history in the RPV, the cavity, the reactor compartments and the containment vessel, post test melt fractions in all locations with size distribution of the debris, video film in the subcompartments and containment (timing of melt flow and hydrogen burning), and pre- and post test gas analysis in the cavity and the containment. The gas analysis allows determining the amount of produced, burned and remaining hydrogen.

Fifteen strain gauge-type pressure transducers (13 Kulite® and 2 Kistler®) are used to measure steam and gas pressures. Twenty-four type-K thermocouples (NiCr-Ni) are installed in the facility. The data acquisition system records data at a rate of 2000 data points per second per channel.

Ten pre-evacuated 500-cm³ gas grab sample bottles are used to collect dry-basis gas samples at three positions, in the upper part of the containment, in the compartment and in the cavity, or in case of the Konvoi geometry in the second compartment. One pretest sample collects background information just prior to the start of the melt ejection. One sample at all three stations each is taken 5 seconds and one 5 minutes after the blow down commenced. Data are obtained for nitrogen, oxygen, hydrogen, carbon dioxide and carbon monoxide by gas chromatography, which have an uncertainty in the order of 5%. The main contributions to the uncertainty are the limit of quantification of the gas samples and the incomplete gas mixing in the vessel. The amount of hydrogen, that is produced and burned during the test, can be determined by the nitrogen ratio method [6, 10]. The data and assumptions required for this method are: (1) the total pretest moles of non-condensable gases must be known; (2) the measured ratios of the pretest and posttest non-condensable gases must be known and (3) it must be assumed that nitrogen is neither produced nor consumed by chemical reactions. The objective of the gas composition measurements and gas analysis is to obtain data on the chemical reactions taking place during the blow-down, that is, the production of hydrogen by the metal-steam reaction and the hydrogen combustion. We cannot distinguish these processes from direct metal-oxygen reactions, but in terms of total energy release, it makes little difference that direct metal-oxygen reaction initially deposits more energy in the debris and less in the gas, because, for small particles that react efficiently, heat transfer is also efficient.

The total debris mass dispersed into the DISCO vessel and the debris mass in specific locations are determined by a post test debris recovery procedure. Loose particles are collected by a vacuum cleaner and weighed separately for each location. The total weight of crusts is determined by pre- and post-test weighing of all parts of the test facility, or if not possible, by removing the crusts from the parts and weighing of them. A post test sieve analysis of the debris recovered from different locations is performed with a standard set of 17 sieves (10 mm to 40 µm). Except for small pieces, crusts are generally not included in the sieve analysis. The information on the droplet size of the melt that has formed a crust is not available. This has to be taken into account when the results of the sieve analysis are evaluated.

B.3. Experimental Results

The initial conditions and the most important results of fourteen experiments performed so far are listed in Table 2, six with EPR, five with P'4, one with VVER-1000, and two with Konvoi geometry. The steam mass in the RPV is determined by the balance between pre- and post test water in the steam accumulator. The temperature in the RPV model vessel is not uniform due to the heating by the thermite reaction at the lower end. Therefore it is not given. The listed RPV pressure is the pressure at melt plug failure.

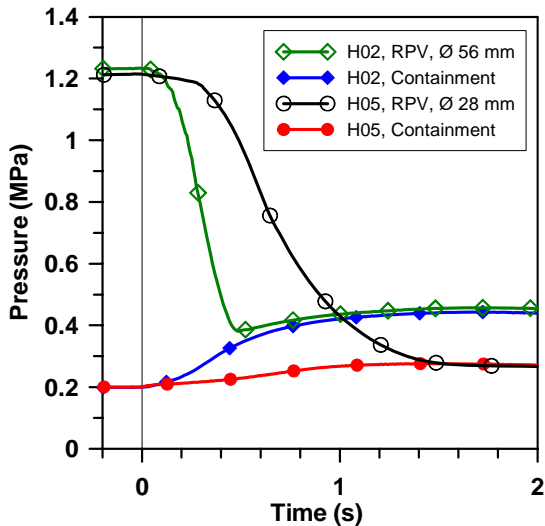


Fig. 9. RPV and containment pressures in EPR geometry

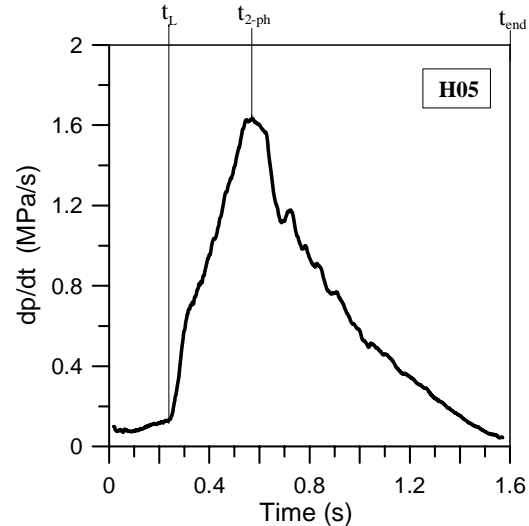


Fig. 10. Gradient of RPV pressure

B.3.1. Results of tests with EPR geometry

Four experiments with EPR geometry were performed with an open path to the containment dome (H01, H02, H04, H06) and two without (H03, H05). Apart from that, tests H02 and H03 had nearly identical conditions, while H05 and H06 had smaller breach sizes, and in test H04 steam was not used, both as driving gas and in the containment atmosphere.

Fig. 9 shows the blow-down and containment pressures for the EPR tests with a scaled 0.5 m and 1.0 meter breach, respectively. From the thermocouple signals in the brass melt plug it can be deduced that the maximum time to fully open the breach cross section is 0.026 seconds. The duration of the blow-down depends on the breach size and is 0.50 seconds for the large breach and 1.60 seconds for the small one. It varies little with the initial pressure. From the pressure gradient three stages of flow can be distinguished (Fig.10). The first stage is the single-phase liquid melt discharge. For test H05, the two-phase melt-steam flow begins at $t = 0.26$ s and lasts until $t = 0.58$ s. From that time on only steam is blown out of the breach at sound velocity (choked flow) until the pressure ratio decreases below the critical value at $t = 0.90$ s.

Fig. 11 shows the pressure rise in the containment vessel and for test H02 the pressure in the cavity. During the ejection of the melt the pressure in the cavity is generally higher, by a maximum of 0.1 MPa, than in the other locations, especially in tests H02, H03 and H04. This hints to a rapid heating of the cavity atmosphere and a flow obstruction by the narrow annular cross section around the RPV. In tests H05 and H06, with the small breach, the melt flow is too small to cause a substantial overpressure in the cavity. Shortly after the end of the single-phase melt ejection the pressure in all locations changes uniformly. The maximum pressure is reached between $t = 1.2$ and 1.75 s (Table 2). Due to heat losses to the vessel walls the pressure decreases again. After approximately 10 s the pressure has dropped to half of its maximum value.

The pressure rise in the containment is highest with an open pit and hydrogen combustion. With a closed pit (H03 and H05) the gas and the debris has to flow first into the sub-compartment and then through relatively small cross sections into the containment. Only 2 % of the melt reached the containment dome. Also, less hydrogen was produced and burned in these cases. In test H04, without steam, no hydrogen effect was present, but with the direct path to the containment open, a large amount of debris was dispersed into the containment, and efficiently transferred heat to its atmosphere.

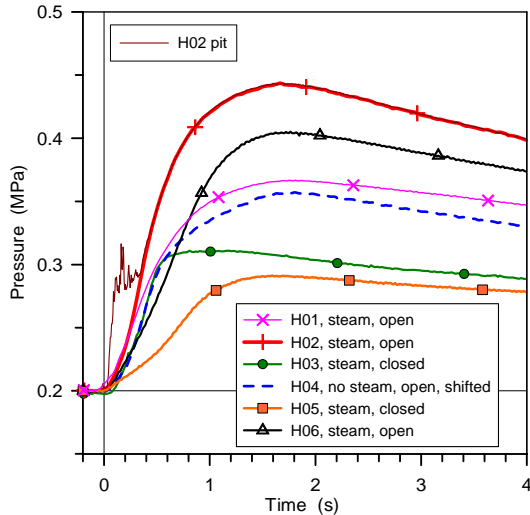


Fig. 11. Containment pressures in EPR tests

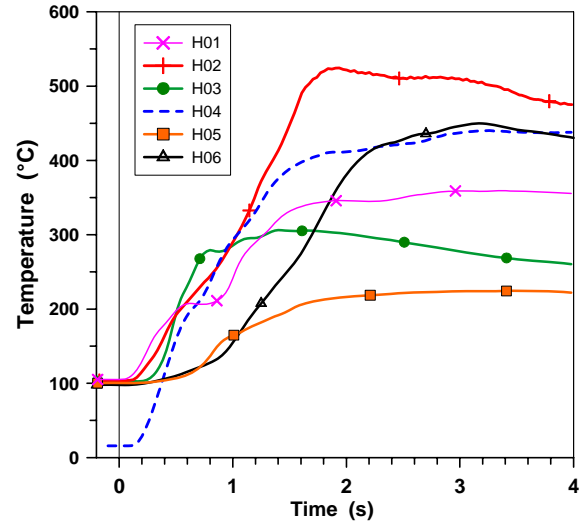


Fig. 12. Containment temperatures in EPR tests

While the pressure is independent from the location in the containment vessel, it is difficult to determine a representative temperature, especially during the first 4 to 10 seconds. Some thermocouples in the compartment and in the lower part of the containment registered very high gas temperatures. Thermocouples close to the compartment exit holes are within or near the hydrogen flame, which could be observed in some tests. Thus, the average was determined by those data, which were not extreme. Those from positions where the flame was burning or near the floor were not considered. Of course, this choice introduces a large uncertainty into the average temperature data. Generally, the gas temperatures in the containment correspond to the pressure rises (Fig.12).

B.3.2. Results of tests with P'4 geometry

In the frame of a French-German cooperation between IRSN and FZK five experiments were conducted with the geometry of the French 1300 MWe P'4 plant, including one test without steam and a nearly inert atmosphere (FH02, funded by the EU Commission, LACOMERA project), and one test without the pit bottom access room and niche (FH05). Three different breach sizes were applied.

The duration of the blowdown (Fig.13) reflects the different breach sizes. Also the pressure in the cavity is a function of the breach size; the peak pressure is higher for larger breach sizes. The lack of the pit bottom access in test FH05 increases the cavity pressure even more.

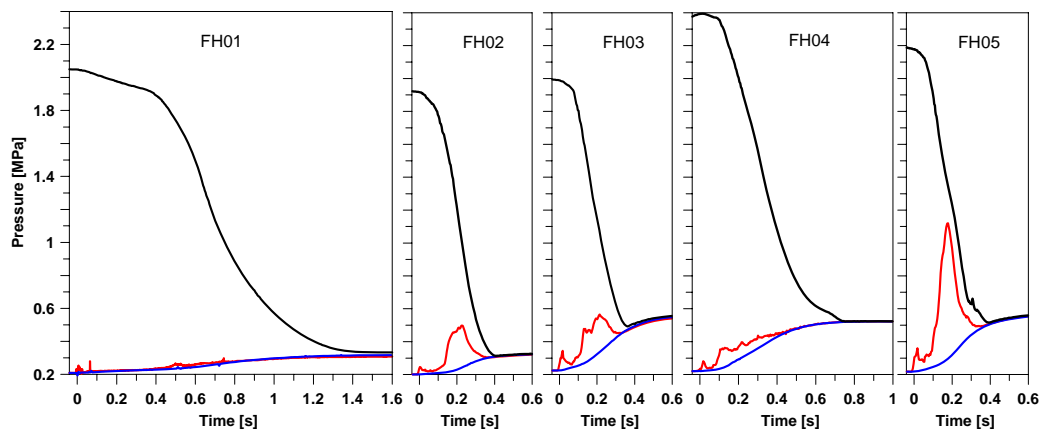


Fig. 13. Pressures in the RPV, the cavity and containment in P'4 tests

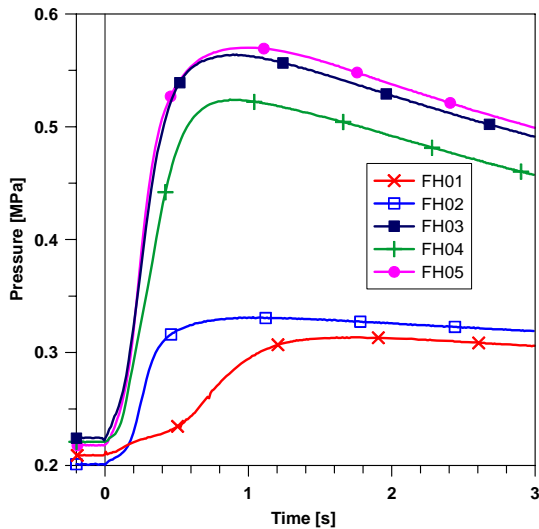


Fig. 14. Containment pressures in P'4 tests

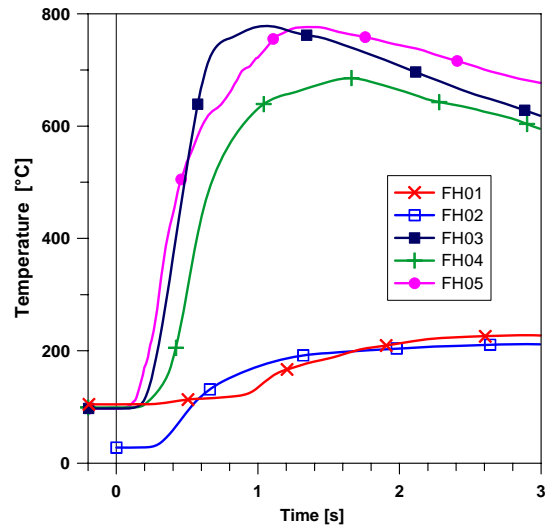


Fig. 15. Containment temperatures in P'4 tests

The debris fraction transported to the containment dome is between 13 and 15 % for the prototypic geometry and 25 % for the geometry without the pit bottom access hatch. A fraction between 13 and 25 % is transported into this small room. Generally the pressure increase is rather high for this geometry (Fig. 14). The average temperatures in the containment dome reach 800 °C (Fig. 15). Apart from the fact that a larger amount of debris is transported to the containment dome compared to the geometry without a direct vertical path, also the height of the lower pit may play a role. In this space the dwell time of steam and melt is longer than in a narrow pit, coupled with flow vortices, and the thermal and chemical interaction of both components is more intense. In test FH01, however, the pressure increase is low. Because of the small breach size more than 70 % of the melt remained in the lower pit and the pit bottom access chamber, where it cannot release its thermal energy to the gas. Only 36 % of the available hydrogen burnt. Test FH02 was conducted with an inert atmosphere, thus the contribution of chemical energy was almost zero and the containment pressure remained low.

B.3.3. Results of tests with VVER-1000 geometry

For the VVER-1000 experiment the breach size at the center of the lower head was small with a diameter of 16.5 mm (reactor scale 250 mm). Due to the small breach size the

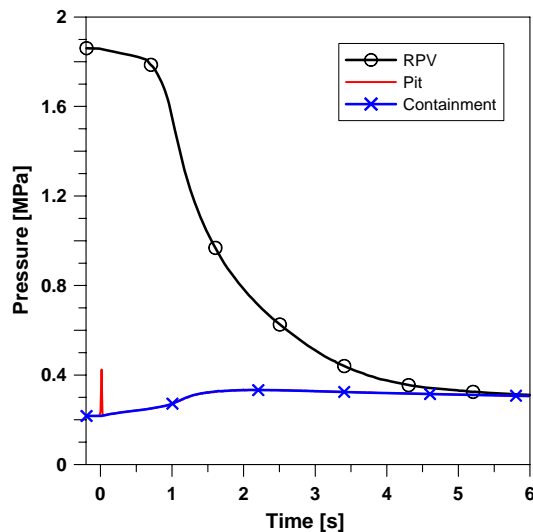


Fig. 16. Pressures in VVER-1000 test

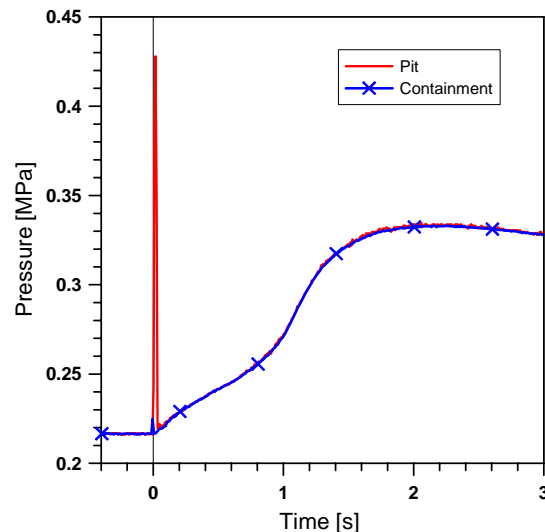


Fig. 17. Pressures in VVER-1000 test

blowdown lasts 5 seconds, that is 75 seconds at reactor scale (Fig.16). Immediately after the melt has entered the reactor pit the pressure rises to 4.4 bars in the pit, and the door in the corridor opens. With the open flow path into the neighboring compartment the pressure drops again. All pressures in the pit, the compartment and the containment rise within 2 seconds to a moderate pressure of 3.3 bars (Fig. 17). The maximum temperature in the containment reaches only 300 °C after 1.5 seconds and remains at approximately 200 °C for a longer time. More than half the melt remained in the reactor cavity (46%) and in the RPV (12%) as crusts, and 40% went through the door into the compartment. Less than 2% reached the containment as fine dust, with a particle mass median diameter of ~0.15 mm. Three quarters of the melt found in the compartment were crusts on the floor and on the wall opposite of the door. The rest had a particle mass median diameter of ~2.5 mm. The venting lines became plugged by frozen melt. The small amount of finely dispersed melt, especially in the containment, is the reason for the low pressure increase, and also for the small hydrogen production by metal oxidation. Only a fraction of 101 moles of the existing iron was oxidized, with part of 43 moles of blowdown steam. 20 moles of hydrogen were produced and 25 moles burned, out of a total of 61 moles.

B.3.4. Results of tests with Konvoi geometry

Two out of planned six tests have been conducted so far with the Konvoi geometry. One test was performed with an open path to the refueling room and one test with this path closed. During the ejection of the melt the pressure in the cavity is higher than in the other rooms (Fig. 18). The maximum pressure difference between pit and the refueling room (subcompartment 2) was 0.153 MPa in both tests, less than the failure pressure of the sealing plates at the vessel support structure (0.2 MPa). For a short time around this pressure peak choked flow between the cavity and the subcompartment occurred.

Fig. 19 shows the pressure increase in the containment in both tests. Surprisingly, the rise is higher in test KH02 with closed flow path through the vessel support. The pressure peak is sharper than that of test KH01. In test KH01 a large fraction of melt was trapped in the small reactor room and the hydrogen content increased to 46 %. This hydrogen did not burn within the first 5 seconds and did not contribute to pressure increase. Also the thermal energy of the melt could not contribute much to pressure increase, because thermal equilibrium in the small room prevented major energy transfer to the atmosphere. In test KH02 the small reactor room was practically passive, only some small particles (150 g) were blown in

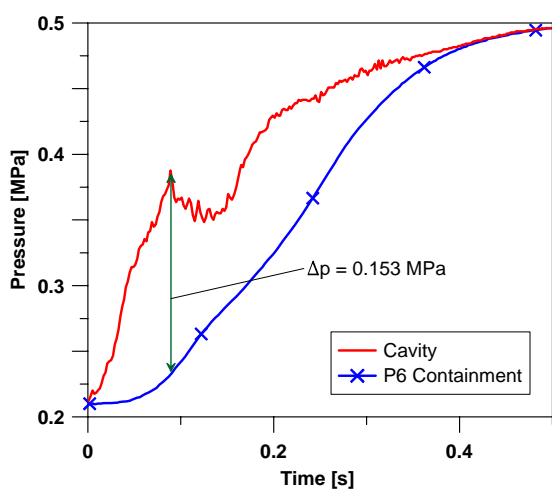


Fig. 18. Pressure in the cavity and containment in Konvoi test

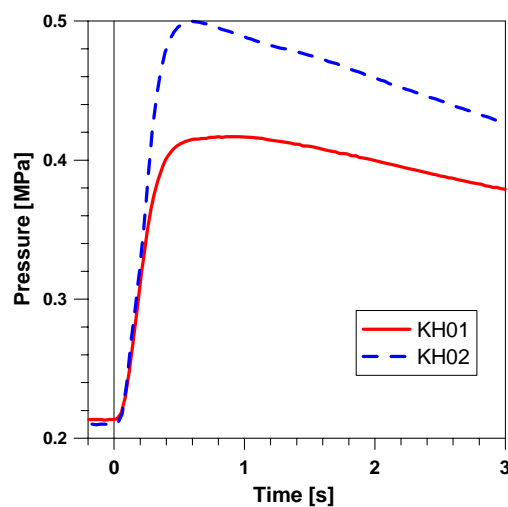


Fig. 19. Containment pressure in Konvoi test

from the containment. On the other hand, more melt entered the subcompartment 1, and because it was the only exit from the pit all gas had to take this way to reach the containment dome. This probably increased the gas velocity and hydrogen burning rate, and thereby the temperature in the containment. In both tests the average temperature maximum in the subcompartment 1 was approximately 1000°C, while in the containment it was higher in KH02 with 500 – 600°C, versus 350 – 450°C in KH01.

Both tests in the Konvoi geometry yielded higher containment pressures than the tests in the similar EPR geometry with ‘closed’ pit (H3, H5). The EPR test H3 had the same breach size as the Konvoi tests. However, the RPV pressure was only 1.0 MPa versus 2.0 in KH02, and the preexisting hydrogen in the containment was 3 % versus 6 – 7 % in KH02. In the EPR test 35 moles of hydrogen burnt, while in the Konvoi test 69 moles burnt. Hence, the higher pressure increase in the Konvoi geometry is not a geometrical effect, but a consequence of different initial conditions.

B.3.5. Analysis of chemical and thermal balances

From the information on the initial masses of gases and melt and the data obtained from the gas samples we can draw conclusions concerning the oxidation of metal and the production and burning of hydrogen. Additionally, the efficiency of the energy transfer to the containment atmosphere by hydrogen burning and melt heat transfer can be assessed by relating to the pressure increase.

In all tests 101 moles of Fe and 4 moles of Al were available (s. Table 1). Complete oxidation of these metals could produce a minimum of 107 moles of hydrogen if there is sufficient steam (107 moles). The maximum available blowdown steam was 50 moles (FH04), while the steam content in the containment vessel was between 300 and 418 moles (Table 2). Oxidation in the containment could also occur with approximately 120 moles of oxygen. Thus, the oxidation in the cavity was limited by the available blowdown steam. The results of the gas sampling indicated generally a higher hydrogen production than moles of blow down steam were available. This means, that oxidation in the containment continued either with

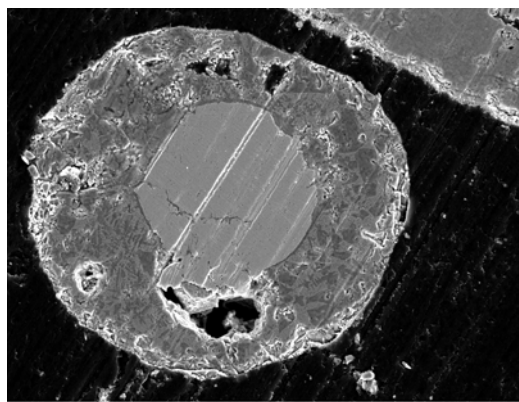


Fig. 20. Debris particle with iron core and oxidic shell

steam or with air. The evaluation method cannot distinguish between a direct reaction of metal with oxygen and the two-tier reaction of metal with steam and a subsequent burning of hydrogen with air. In the first case less hydrogen would be produced and burned than in the second case, but energetically both cases are identical. In any case, according to the measured decrease of oxygen in the containment and the hydrogen balance, less than half of the initially available metal was oxidized or less than half of the possible hydrogen was produced. A chemical analysis of the debris showed that even small particles in the sub-millimeter range were not oxidized throughout, but often contained an iron core (Fig. 20).

With the exception of two tests the amount of hydrogen that burnt was larger than the amount of hydrogen initially available. The EPR test H05 is different from the rest by the combination of a closed cavity and a small breach size, while the P'4 test FH01 has a smaller breach size also and a smaller initial hydrogen content in the containment than the other P'4 tests. The fraction of hydrogen that burnt relative to the total amount available is between 0.36 and 0.84. The theoretical possible pressure rise resulting from the energy release by hy-

drogen burning can be obtained by combining the caloric equation of state with the ideal gas law,

$$\Delta p = \frac{\kappa - 1}{V} \Delta Q_H,$$

with κ the ratio of gas specific heats and V the containment volume ($V = 13.75 \text{ m}^3$). The combustion of the hydrogen releases $\Delta Q_H = 242 \text{ kJ/mol}$. The steam in the containment is at saturation and does not quite obey the ideal gas law. Furthermore, there is always some fog which consumes energy for vaporization. This theoretical pressure rise is in all case larger then the measured one, although the contribution by heat transfer from the debris is not included.

For the assessment of the energy transfer from the melt to the atmosphere we will assume that only the fraction of melt that has a diameter smaller 2.5 mm can release its energy within the DCH time scale. The specific thermal energy of the melt used in the experiment is given by [14] with $\Delta e_{\text{therm}} = 0.182 \text{ MJ/mol}$. Only a fraction of thermal energy can be transferred from melt debris to the atmosphere before debris-gas thermal equilibrium is achieved. This fraction is given by the expression $1/(1+\Psi)$ according to Pilch [15], with the heat capacity ratio Ψ , of the debris mass to that of the containment atmosphere. Locally this ratio can be quite large, but referred to the whole of the containment it is small. In this rough estimate of maximum pressure increase we will use the total amount of the containment atmosphere, which is approximately $N_{\text{atmo}} = 1000$ moles and the mass fraction of melt that was dispersed:

$$\Delta p = \frac{\kappa - 1}{V} \frac{\Delta e_{\text{therm}} N_m f_d}{1 + \Psi}$$

with $\Psi = N_m f_d C_{\text{pm}} / N_{\text{atmo}} C_v$.

N_m is the number of moles of melt, f_d is the dispersed fraction with debris diameter smaller than 2.5 mm, C_{pm} is the specific heat of the melt with $C_{\text{pm}} \sim 82.8 \text{ J/mol/K}$, and C_v is the specific heat of the atmosphere with $C_v \sim 28 \text{ J/mol/K}$ ($C_{v \text{ air}} = 20.8 \text{ J/mol/K}$) ([6],[14]). The heat capacity ratio Ψ lies between 0.15 and 0.25 for the experiments with a steam atmosphere and is 0.50 for test H04, which had a high dispersed melt fraction and an air atmosphere in the containment. The theoretical pressure increase due to heat transfer alone in most cases is smaller than the measured one.

The total DCH-efficiency is the ratio of the measured pressure increase to the sum of both theoretical pressure rises, due to combustion and heat transfer. These values lie between 0.30 and 0.38 for the EPR geometry, between 0.40 and 0.58 for the P'4 geometry, at 0.65 for the VVER-1000, and between 0.39 and 0.47 for the Konvoi geometry (excluding tests without steam).

This short analysis can be refined following the approach of the 'Two Cell Equilibrium' model by Pilch [15], taking into account the compartmentalization of the reactor plants and heat losses. It would give further indications for mitigating effects concerning the peak containment pressure.

Annotations to Table 2:

- 1) Minimum annular flow cross section between RPV and cavity wall
- 2) Flow area around main cooling lines
- 3) Direct flow path to containment dome; in case of Konvoi, to refueling room above RPV
- 4) Flow area to room at pit bottom level, (initially closed at VVER-1000)
- 5) Due to small flow cross section upstream at vessel support, size of this flow cross section is irrelevant
- 6) Transported to the refueling room above RPV
- 7) Data determined from gas samples are not always consistent with added hydrogen mass

Table 2: Initial conditions and summary of results of all DISCO-H experiments

Plant type Scale	EPR 1:18					1300 MWe P'4 1:16.4					VVER Konvoi 1:15.2 1:18.5				
	H01	H02	H03	H04	H05	H06	FH01	FH02	FH03	FH04	FH05	L2	KH01	KH02	
<i>Initial Conditions</i>															
RPV pressure	MPa	0.77	1.22	1.25	0.89	1.21	2.16	1.62	1.92	1.98	2.39	2.18	1.86	2.57	2.00
RPV steam	g mol	7.0	15.0	16.0	0	20.7	34.9	20.1	0	34.6	49.8	39.2	43.0	28.3	33.3
RPV nitrogen	g mol	2.0	2.0	2.0	12.0	2.0	3.2	1.8	21.7	1.6	1.8	2.0	1.8	2.1	2.1
Hole diameter	cm	5.6	5.6	5.6	5.6	2.8	2.8	3.0	6.0	6.0	4.2	6.0	1.65	5.6	5.6
Scaled hole dia.	m	1.0	1.0	1.0	1.0	0.5	0.5	0.5	1.0	1.0	0.7	1.0	0.25	1.0	1.0
Compartment volume	m ³	1.74	1.74	1.74	1.74	1.74	1.74	2.45	2.45	2.45	2.45	2.45	2.45	2.78 0.146	2.78 0.146
Flow path															
around RPV ¹⁾	cm ²	212	212	212	212	212	212	110	110	110	110	110	15	315	315
at nozzles ²⁾	cm ²	308	308	308	308	308	308	393	393	393	393	393	n/a ⁵⁾	80	80
to cont. vessel ³⁾	cm ²	520	520	0	520	0	520	114	114	114	114	114	n/a ⁵⁾	73	0
to pit room ⁴⁾	cm ²	-	-	-	-	-	-	60	60	60	60	0	246	-	-
Vessel pressure	MPa	0.21	0.21	0.20	0.10	0.20	0.21	0.21	0.20	0.22	0.22	0.22	0.22	0.21	0.21
Vessel temp.	K	376	376	373	293	374	375	375	303	373	368	367	369	376	372
Vessel gas	g mol	908	908	889	570	898	924	908	898	993	977	988	967	947	942
Gas composition in vessel															
Steam	mol%	36.6	36.6	34.2	0	33.5	35.8	46.0	0	36.0	37.4	36.9	37.8	35.1	34.5
N ₂	mol%	47.4	47.4	49.2	78.0	49.7	47.7	39.9	96.8	45.4	44.4	45.6	45.5	46.4	46.9
O ₂	mol%	12.8	12.8	13.2	21.0	13.4	12.8	10.7	3.2	12.2	11.9	12.3	12.2	12.5	12.6
H ₂	mol%	2.6	2.6	2.7	0	2.9	3.1	2.8	0	5.8	5.7	4.6	3.9	5.4	5.4
other	mol%	0.6	0.6	0.6	1.0	0.6	0.6	0.5	0	0.6	0.6	0.6	0.6	0.6	0.6
<i>Experimental results</i>															
Melt transport fractions															
in cavity		0.65	0.40	0.54	0.25	0.62	0.51	0.46	0.39	0.45	0.48	0.46	0.53	0.14	0.48
containment		0.24	0.50	0.02	0.66	0.02	0.36	0.13	0.15	0.15	0.13	0.25	0.01	0.08	0.03
compartment		0.12	0.10	0.44	0.09	0.36	0.13	0.16	0.28	0.24	0.26	0.29	0.46	0.44	0.48
pit room		-	-	-	-	-	-	0.25	0.18	0.17	0.13	-	0.34 ⁶⁾	0.01 ⁶⁾	
particle diam. < 2.5 mm		0.193	0.427	0.202	0.510	0.075	0.278	0.135	0.218	0.208	0.176	0.215	0.047	0.227	0.208
Sieve analysis: debris fractions smaller 10 mm in															
containment		0.78	0.90	1.00	0.91	1.00	0.86	0.76	0.56	0.81	0.83	0.48	0.83	0.90	0.88
compartment		0.86	0.97	0.91	0.99	0.55	0.71	0.72	0.76	0.77	0.72	0.89	0.19	0.64	0.70
Sieve mass median diameter (SMMD) of particles < 10 mm in															
containment	mm	1.1	1.3	0.16	1.4	0.15	1.4	0.5	0.3	0.4	0.3	0.2	0.2	0.8	0.1
compartment	mm	2.1	2.8	3.5	1.5	4.8	2.6	2.3	1.3	2.0	2.0	2.9	2.5	1.7	2.0
total	mm	1.4	1.5	3.1	1.4	4.5	1.5	1.5	0.8	0.9	1.0	1.4	2.0	1.6	1.9
Hydrogen															
pretest ⁷⁾	g mol	24	26	27	0	29	35	38	0	67	55	48	41	60	69
produced	g mol	no data	54	33	n.d.	32	39	40	15	44	48	42	20	37	33
burned	g mol	n.d.	66	35	n.d.	26	49	28	7	83	75	75	25	53	69
post-test	g mol	n.d.	14	25	n.d.	35	25	50	8	28	28	15	36	44	33
Fraction burned		-	0.83	0.53	-	0.43	0.66	0.36	0.46	0.75	0.73	0.84	0.41	0.55	0.67
Δp _{max} meas. in containment	kPa	170	236	114	156	90	194	104	130	338	302	351	120	205	290
Time of p-peak	s	1.75	1.75	1.20	1.75	1.75	1.75	1.57	1.00	0.85	0.80	0.94	2.10	0.93	0.60
<i>Analysis</i>															
Δp _{max} H ₂ burn	kPa	-	450	255	310	203	342	173	43	510	460	463	153	364	462
Δp _{max} HT melt	kPa	125	250	130	294	51	173	90	142	135	115	139	33	134	152
Δp _{max} total	kPa	-	700	385	604	254	515	262	185	644	576	602	185	528	614
DCH-efficiency			0.34	0.30	0.26	0.35	0.38	0.40	0.70	0.52	0.52	0.58	0.65	0.39	0.47

C. CODE MODELING

The first key point for any ambitious approach of analytical modeling of the very dynamic and complex phenomena related with DCH is the description of the melt fragmentation in the reactor cavity and the dispersal of fragmented melt fractions within the rooms of the reactor plant. The two important other issues, namely oxidation and combustion, depend closely on the fragmentation and transport characteristics. There are many circumstances which contribute to the enhanced complexity of this process and make realistic analytical descriptions very difficult:

- During the period of blowdown from the RPV the regimes of single-phase liquid flow (corium melt), two-phase flow (melt and steam) and single-phase flow (steam) will establish in succession to each other. The need for a precise description is not evident.
- At least three phases have to be considered for a proper simulation of the phenomena in the reactor cavity: i) A continuous liquid phase (melt jet/film), ii) a continuous gaseous phase (atmosphere/steam) and iii) a dispersed liquid phase entrained in the gaseous phase (melt droplets). The process of solidification of the melt introduces additional solid phases with consequences on the fragmentation/entrainment processes.
- The process of melt entrainment into the gas flow is very much dependent on local material properties and local phase velocities. Due to the geometric details of the reactor cavity, the flow patterns may be very complex and the related local properties/quantities are not known with sufficient precision.
- There is a dynamic feedback between the fragmentation process and the pressure distribution among the rooms in the containment. Higher gas velocities tend to entrain smaller melt droplets, which affect via energetic interactions the pressure distribution along the flow direction considered.

Due to this high complexity of the involved processes appropriate simplifications are necessary in the analytical approaches and several approaches with different degree of simplifications have been proposed:

Models based on a control-volume discretisation scheme for reactor plant/containment in combination with a lumped parameter formulation of the corresponding thermo-hydraulic states. Well-known models belonging to this subgroup are the system codes CONTAIN [16], MELCOR [17], MAAP [18], COCOSYS [19] and ASTEC [20]. In such approaches it is generally possible to account for the specifics of a certain room (e. g. in terms of the configuration and properties of heat structures, or in terms of the room's geometric dimensions representing maximum free path lengths for particle flow etc.). Usually the source for entrained melt is mapped here to a special "cavity" cell. For the cavity cell a correlation for the entrainment rate is applied to calculate the mass of entrained melt per time unit in dependence of the melt availability in the cavity (resulting from the discharge of the melt from the RPV) and of the properties of the gas flow. Because of the lumped parameter formulation of the codes the gas velocity considered for the entrainment rate correlation has to be averaged from the inlet/outlet volume fluxes calculated for the cavity cell. While the codes MELCOR, MAAP and ASTEC take into account only a very simplified balance of the entrained melt requiring additional input parameters like the melt distribution in the different containment zones and the average flight time of airborne droplets, the codes CONTAIN and COCOSYS use a more mechanistic transport model for airborne melt fractions.

Recently, with the development of computer capabilities, a new approach has been elaborated in the frame of SARNET, using models based on numerical solvers for the relevant transport equations of continuum mechanics with a sufficiently fine resolution of the numerical grid to take relevant geometrical details into account. The codes used for this purpose are AFDM [21] and MC3D [22]. These codes use methods of computational multi-fluid dynamics (CMFD) to solve the hydrodynamic equations for the multi-phase and multi-dimensional flow in the reactor cavity where the process of melt entrainment takes place. The continuous liquid melt (i.e. the jet from the RPV and the film on the basemat of the cavity), the continuous atmosphere above the melt and the dispersed melt droplets carried by the gas flow are considered as separate phases. Calculations are performed using 2D or 3D grids. However, the fragmentation phenomena themselves, in terms of field exchanges or simply variation of surface area, have to be described by dedicated models. In AFDM a similar correlation for entrainment rate as for the lumped parameter codes is used, but detailed data with a higher spatial resolution are taken into account by AFDM [13]. In MC3D the processes of fragmentation and coalescence are modeled to calculate the transition of a specific melt volume from the continuous liquid phase to the dispersed liquid phase (fragmentation) and vice versa (coalescence). In MC3D fragmentation is referred to a Kelvin-Helmholtz instability approach and coalescence is referred to impact processes between droplets or between droplets and continuous liquid.

Regarding modeling, the activity in SARNET was oriented towards the analyses and improvement of the lumped-parameter models, particularly ASTEC and COCOSYS. For this purpose, a preliminary work was engaged:

- Comparison of the lumped-parameter models used in SARNET community, namely ASTEC, CONTAIN and MAAP in terms of models and results compared to experimental data (DISCO).
- Continuous improvements of the CMFD codes AFDM and MC3D and analyses of the results in view of providing an improved comprehension of the main phenomena.

In the following of this section there is at first a summary of the analysis made from the comparison of the lumped-parameter codes. Then the major findings gained with the development and use of MC3D are outlined. Finally, the model choices and lines of development for COCOSYS will be given with a particular attention on the qualification regarding DISCO experiments.

C.1. Conclusions from comparative analyses between lumped-parameter model approaches

In the frame of SARNET it was agreed to perform comparative analyses with available codes which include integrated models dedicated to DCH evaluations and which are in use at the participating organizations. The RUPUICUV (IRSN) module of ASTEC is one of them. The two other tools used in the SARNET community are CONTAIN/COCOSYS (GRS) and MAAP (EDF). The analyses were however performed without taking account of the chemical aspects, with application to the DISCO FH02 test (P'4 geometry) which was done with a neutral environment (no vapor or oxygen) [23].

ASTEC and MAAP are, regarding DCH, relatively similar, using a very simple approach, with a model for melt dispersion based on correlations for the integral fraction of dispersed melt. It can be noticed that currently the heat transfer between the melt and the gas in

ASTEC is modeled through an interface module (called CORIUM) between RUPUICUV and CPA (containment module). CORIUM acts like a source term for CPA. This was recognized as a weakness and there are currently considerations to improve this by the addition of a melt drop field in CPA. CONTAIN is a bit more complex and includes several models for melt dispersion, reflecting both an important activity and an important uncertainty. Some models are based on correlations for entrained fraction of melt, but the one used by GRS is based on a correlation for entrainment rate using "local" and temporal properties.

The analyses performed show that large uncertainties and knowledge gaps exist both in understanding and assessing all phenomena associated with DCH. It is therefore a prerequisite for any model-development to clearly understand the main processes and possible interactions in detail.

The crucial point for the usage of the simplified analytical models and of the system codes is the application of correlations for the entrainment rate as function of averaged quantities with no or only limited impact of geometrical characteristics. First of all it was found that correlations are usually difficult to understand and complex to use. As the models are supposed to work for a wide range of geometrical characteristics some geometrical details must be provided. In most cases the user has some unexpected freedom in the use of the models. Potential errors are made by estimating an average gas velocity for entrainment from bulk quantities like the inlet/outlet volume fluxes. Further, the size of the interface between melt and gas must generally be supplied in the input. Additional coefficients in the correlation for the entrainment rate must compensate here for all other (geometrical) influences which are not considered in these approaches.

Based on the comparative analyses it is expected that a simplified approach is not able to capture all relevant physics independently of the geometry. This expectation includes that – in system codes – the model or at least the sets of parameters must be taken as geometry-specific. Calculation results performed with several codes for the experiment FH02 in the geometry of the P'4 reactor clearly demonstrate model deficiencies, leading to unsatisfactory results due to arbitrary fittings. Further analyses work in SARNET shows that hydrogen production and combustion as a result of droplet fragmentation and enhanced oxidation is not correctly captured and calculated in the codes.

C.2. Analyses performed with MC3D with regard to the melt dispersion

The objective of the development of multidimensional multiphase flow codes as MC3D is multi-fold:

- improve the comprehension of the phenomenon;
- supply additional data if the qualification is proven;
- improve confidence regarding extrapolations to reactor material and scales;
- assess the possibility of the phenomenon for new or modified geometries.

It is to be recalled that currently MC3D does not compute combustion. Because of that the complete process cannot be evaluated. Also, the oxidation model is still rather parametric and needs refinement. However, both effects are not expected to modify strongly the melt entrainment which was the focus of the studies made up to now with MC3D.

C.2.1. Main achievements in the improvement of comprehension

Figure 21 provides a visualization of the main characteristics of the codes. The melt is computed with two fields having their proper mass fraction moment and energy, one being continuous, representing for example jets, pools or films, modeled with a VOF-PLIC method, one being dispersed, representing small drops. The drops are created by a fragmentation model using local quantities and properties. The figure shows both fields superimposed (the drop field is not visible where the volume fraction is lower than 1%).

One of the first achievements has been to show the code ability to reproduce satisfactorily the different flow patterns at the breach. The vessel depressurization is well calculated with no artifice even during the complex 2-phase flow stage.

It has also been found that melt entrainment out of the pit occurs mainly during the gas single-phase flow stage at the breach. During the 2-phase flow stage, the inertia of the melt reduces strongly the gas velocity. Thus, it is likely that, for simplified models, a rough model for the melt ejection is sufficient. The melt is however for a large part finely fragmented at the breach. But it hits rapidly the wall or the floor and re-coalesces. Then, the melt ejection necessitates a second process of fragmentation in the pit. In MC3D, this second fragmentation occurs along the wall where a melt film is formed and entrained upward. This can be very difficult to compute with a simple model. It is quite easy to compute the gas flow in the pit in the absence of melt. However, the presence of the melt affects strongly the gas flow patterns with, in particular, a strong reduction of the velocity. We find from the calculations that the average drop diameter in the pit is in the range of millimeters, i.e. rather large (except for the particular case of water flow). This is not in the range of the experimental observations where very fine particles are found in the dome. This is due to a third process of re-coalescence/fragmentation, occurring in the upper part of the pit. The final drop diameters are in fact correlated with the velocities at the particular flow entrance areas for each particular compartment. The experimental results on this point give only very partial information on the fragmentation processes, particularly those occurring in the pit.

The fragmentation at the breach has nevertheless some importance of the flow characteristics regarding thermal and chemical processes. Fig. 22 gives a visualization of the thermal field in an example of calculation (same as Fig. 21). The background color is relative to the gas temperature. During the single-phase melt flow, the fragmentation at the jet is very weak due to the very short traveling time¹. The pit temperature is not affected. As soon as the flow becomes two-phase, the high velocity entrains a high heat transfer and the pit atmosphere is very rapidly heated at temperatures close to the melt one. This is accompanied by a sudden pressurization in the pit (see for example figure 13 for experimental confirmation). However, the flow at the breach becomes progressively single-phase and the pit then starts to cool down again.

The same process is observed with the gas composition. Due to the high temperature, the oxidation time scale is very short. The fragmentation at the breach leads to a strong oxidation and the gas composition is strongly affected.

Overall, the process of melt entrainment occurs with extremely transient conditions regarding the gas composition, temperature and pressure, conditions which are of course essential in the computation of the fragmentation and entrainment processes. It is very unlikely that an analytical simplified model could handle adequately such variations. However, the calculations suggest that the global results are not too strongly affected by these transient processes.

¹ In the experiment and probably also in the real case, there is an additional fragmentation at the edge of the breach which is not accounted for in MC3D. This is of small overall influence.

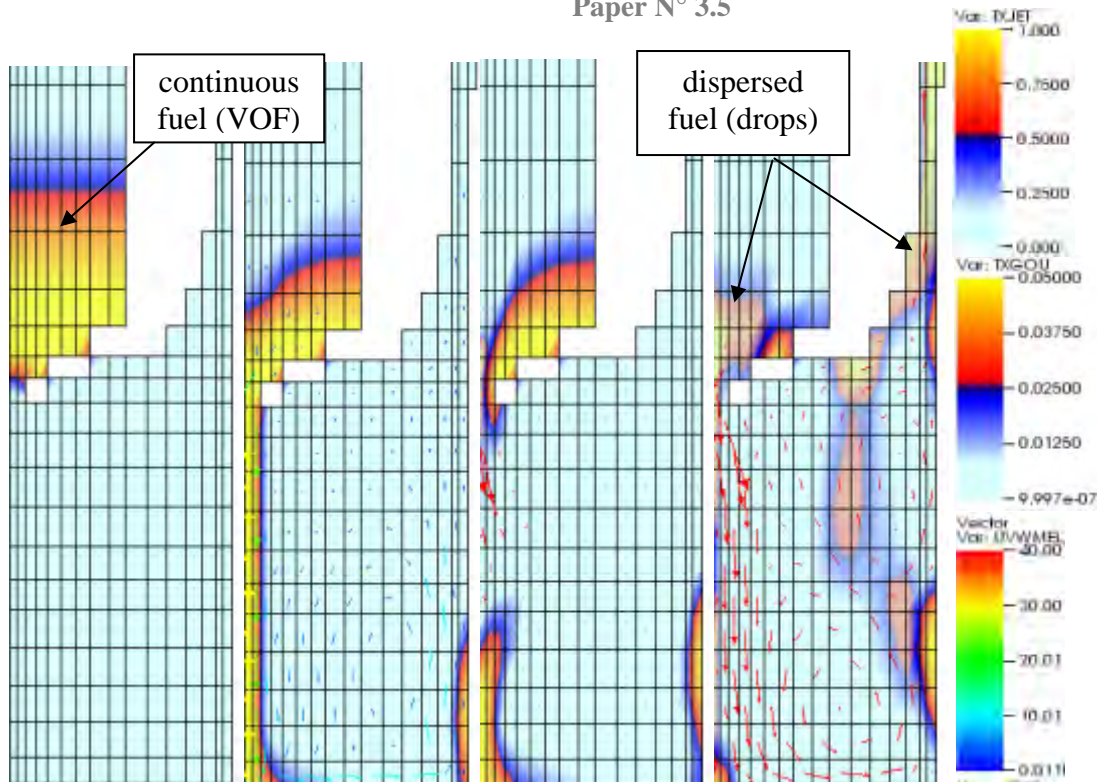


Fig.21. Visualization of melt ejection fragmentation and upward dispersion in a typical simulation of DISCO integral test ($P_v = 19$ bar, $D_b = 30$ mm, $\text{Al}_2\text{O}_3\text{-Fe}$ thermite at 2500 K, vessel gas: steam). Legend: top: continuous fuel field volume fraction, middle: fuel drop volume fraction, bottom: drop velocity (m/s, limited to 40 m/s).

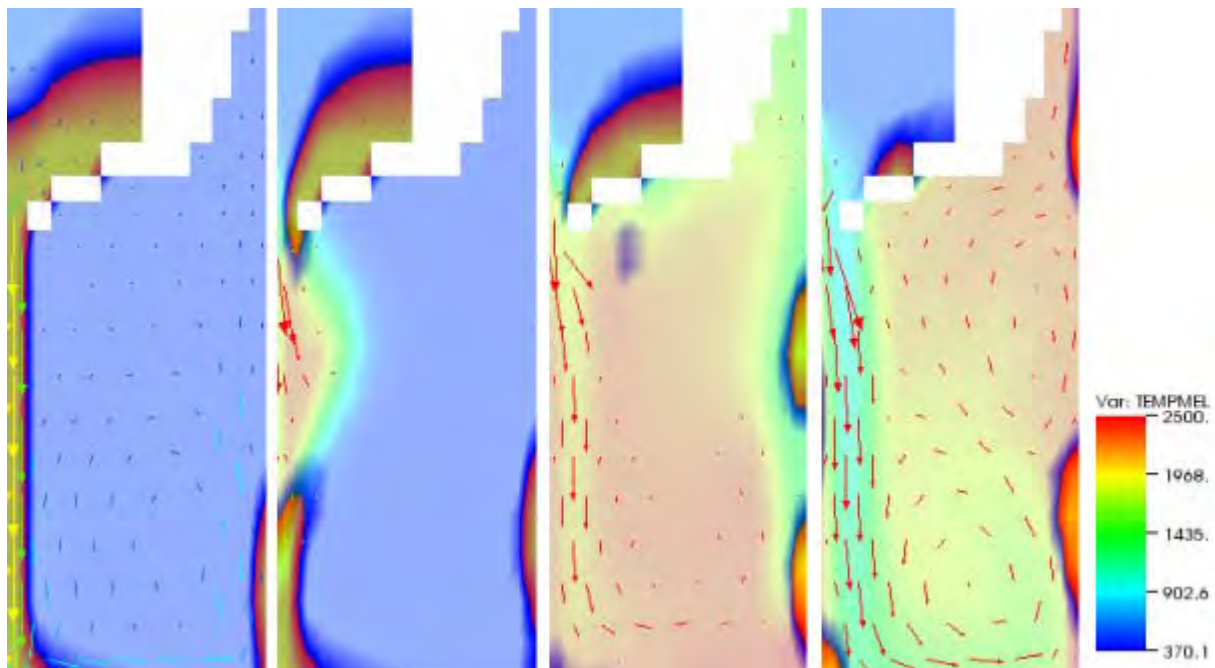


Fig. 22. Visualization of gas temperature during the phase of melt ejection (same calculation as in Fig. 21). Legend: gas temperature (K), see also Fig. 21 for continuous melt volume fraction and drop velocity.

It is likely that there exist compensation effects so that the major global parameters (i.e. gas density and velocity) are not strongly modified by the thermal and chemical processes. This point is however still to be demonstrated on a theoretical ground.

C.2.2. Geometrical effect

Depending on the reactor geometry, there are several geometrical effects that need to be studied with attention.

The first effect is common to all geometries and pertains to the scaling. It is already well-known that the scaling has no effect on the pure gas flow patterns. Also, as the velocities are unaffected, and as the duration of the phenomenon scales with the time for RPV depressurization, it is found that the time scale for the phenomenon is the same as the length scale. In reactor scale this gives more time for fragmentation effects. Also, theoretically, a smaller scale induces an enhancement of frictions with walls and heat losses with structure (increased area/volume ratio). However, the friction effects seem to have a small impact at the DISCO scale already. The question of heat losses is currently under investigation and must include the question of combustion modeling. It is likely that the DISCO scale is not conservative regarding the pressurization. Regarding the dynamical aspects, we find with MC3D that only minor changes occur in calculations at reactor scale. During the first single-phase melt ejection at the breach there is more time for fragmentation, as the velocities are the same regardless of the scale and the distance to the floor increases. In most cases, the jet is completely fragmented before hitting the floor. However, as for the two-phase flow, this has no real effect. Also, the film along the wall has a smaller relative extend and fragmentation occurs in lower parts of the pit. Overall, the dispersion is noticeably retarded but, the overall effect is largely covered by the various uncertainties.

For the particular case of large pits with an access path, as for the P'4 reactors, the supplementary exit should have an important impact. However, based on MC3D calculations it was suggested in a preliminary analysis [24] that, in the particular case of P'4 reactor, this path had effects only on the maximum possible amount of melt dispersed upwards from the cavity. Some additional cold experiments made with DISCO (with Wood's metal) have confirmed this important finding. This will be demonstrated in the next section.

The last important geometrical point regards the separation of the melt that occurs in the upper part of the pit. This involves very complex processes due to the complex geometries. Here the melt experiences a new re-coalescence process followed by a new fragmentation. A modeling of this is theoretically possible, but needs a precise 3D description and consequently large CPU times. This is currently under investigations.

C.2.3. Melt dispersal correlation

As a supplementary possible strategy for the improvement of system codes, correlations for melt entrainment rate could be deduced from calculations with these CMFD codes. One could either directly introduce this correlation into the lumped-parameter model (strategy for ASTEC), or test thoroughly the system-code against it (strategy for COCOSYS).

This is one of the achievements gained from the use of MC3D with application to the French P'4 reactor. At first, we derive the correlation for the 2D case and look for its applicability for 3D experimental results. We also restrict the analysis to the upward dispersed fraction. As already said, the separation of the melt between the dome and sub-compartments will necessitate additional analyses.

The starting point is the idea that there exists a feedback between entrainment and fragmentation. Balancing the cohesion and fragmentation forces on one side, and friction and gravity forces on the other side, one can obtain a relation for the relative velocity (or free fall velocity) Δv between the gas and the drops :

$$\Delta v^2 \approx \sqrt{\frac{4}{3} \frac{\sigma \text{We}_{\text{eq}} \rho_d}{C_{d0} \rho_g^2} g}$$

Here, We_{eq} represents an equilibrium Weber number, i.e. the mean averaged Weber number of the drops at free fall. From experiments [25] it was found that this equilibrium Weber number is noticeably smaller (between 1 and 6) than the classical critical Weber number (equal to 12). In the MC3D calculations, a value of 3 seems to give the best compromise. C_{d0} is the drag coefficient for a single drop. The above expression allows defining a dimensionless number called the Kutadeladze number:

$$K = \frac{\rho_g v_g^2}{\sqrt{\sigma \rho_d} g}$$

The main idea of the proposed correlation is to make the hypothesis that the dispersed fraction can be expressed by this number. The dispersion is a function of the mass flow rate and thus we will seek for a relation using the square root of the Kutadeladze number, i.e.:

$$F_d = f(\sqrt{K})$$

The problem is to express the gas velocity and density. If we assume that the pit is very rapidly in a quasi-steady state, then the mass flow rate at the annular space equals the one at the breach. The latter is, for all cases of interests, supersonic. We then arrive at the following expression:

$$F_d = f\left(0.56 \frac{A_b}{A_a} P_v \sqrt{\frac{\gamma M_m}{RT_v}} (\sigma \rho_d g)^{-1/4} \sqrt{\frac{1}{\rho_g}}\right)$$

where:

- P_v and T_v are the initial pressure and gas temperature in the RPV.
- M_m and γ are the molar mass and adiabatic constant of RPV gas
- A_b and A_a are the flow cross section of vessel breach and annulus, respectively.

The gas density is not expressed. However, we find that an arbitrary reference value can be used. We also find that the role of the cross section of the breach is not so important. This can be understood if we notice that the available time for entrainment is the vessel depressurization time. In that case, the gas blow down time is inversely proportional to the breach area. Overall, we find that the dispersed fraction can be correlated as:

$$F_d = f\left(0.56 \left(\frac{A_b}{A_a}\right)^{1/4} P_v \sqrt{\frac{\gamma M_m}{RT_v}} (\sigma \rho_d g)^{-1/4} \sqrt{\frac{1}{\rho_0}}\right),$$

where ρ_0 is a reference density kept to have a dimensionless expression, taken to be 1 kg/m^3 . This dependency has been assessed against a large number of calculations with MC3D and the experimental data available (Fig. 23). The calculations are done with a very rough mesh, so that the computations are fast. One can notice the considerable scatter of the results. This is due to the rough mesh and to some intrinsic modeling features such as the VOF-PLIC method, which needs a fine mesh for real accuracy. However, we can notice that the tendency applies as well for cold water test as for iron-alumina hot tests.

The correlation itself reads

$$F_d = \frac{F_{d,max}}{2} \left\{ 1 + \tanh \left[A * \log \left(\frac{\sqrt{K^*}}{\sqrt{K_{50}^*}} \right) \right] \right\}$$

with: $\sqrt{K^*} = \left\{ 0.56 \left(\frac{A_b}{A_a} \right)^{1/4} P_v \sqrt{\frac{\gamma M_m}{RT_v}} (\sigma \rho_d g)^{-1/4} \sqrt{\frac{1}{\rho_0}} \right\}^2$,

$\rho_0 =$ reference density = 1 kg/m³,

$\sqrt{K_{50}^*} = 170$, $A = 5.$, $F_{d,max} = 0.9$.

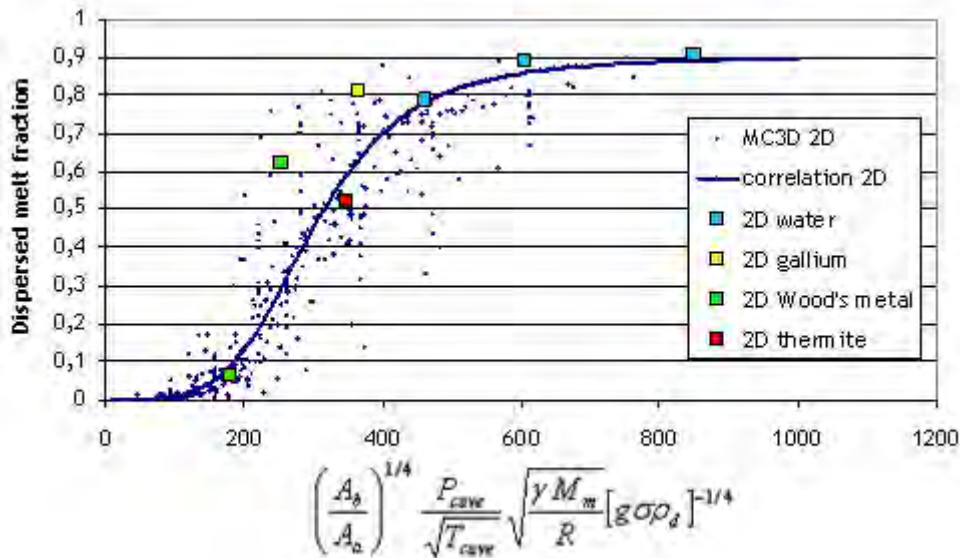


Fig.23. Functional dependency of the dispersed fraction for the restricted case of the DISCO P'4 2D experiments

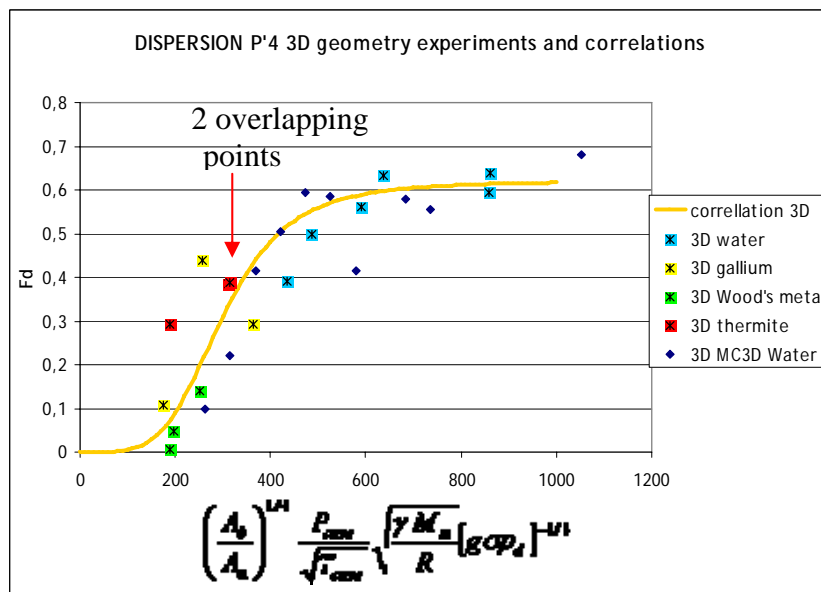


Fig. 24. Comparison of the correlation with all available 3D experimental DISCO data for the P'4 geometry, same parameters as 2D correlation except maximum dispersion.

Although the code can compute 3D situations quite satisfactorily [24] we did not make sufficient calculations to assess the correlation. But we have sufficient experimental data for this purpose. Figure 24 shows this comparison, including some MC3D results. The correlation here is exactly the same except that $F_{d,max} = 0.6$. Note the two overlapping iron-alumina (thermite) results (with different initial conditions). The transition between no entrainment and full entrainment is rather sharp.

To complete the findings, it should be noticed that the calculations show a small but noticeable difference in behavior between cold and hot experiments. Also, there is a similar difference when we use the real scale.

C.3. Analyses performed with COCOSYS with regard to the integral effect of DCH on containment thermal-hydraulics

Recently the containment code system COCOSYS has been extended with a module for the simulation of phenomena during melt release from the reactor pressure vessel (RPV) into the containment. This model extension is closing the gap of models in the analysis codes of GRS between the in-vessel processes, which lead to the meltthrough of the reactor pressure vessel, and the simulation of melt behavior outside of the RPV (melt spreading/relocation, MCCI).

The model extensions were based upon intensive experiences in application of the U.S. containment code CONTAIN. Hence, in COCOSYS many detailed models are implemented in close analogy to CONTAIN with selective simplifications and improvements. Finally a basic assessment of the new module COCOSYS-DCH was performed, including detailed post-test calculations of experiments in the DISCO and in the Surtsey facility, comparison with CONTAIN in a benchmark for the experiment DISCO-FH02 and a comparison with CONTAIN for a plant case (Sequoyah).

The predictive capability of the code COCOSYS regarding the most important quantities related to the impact of DCH is checked here in blind calculations for four different experiments (FH01, FH03, KH01, KH02) in two different geometries (P'4 reactor and Konvoi plant).

C.3.1. Fixing of a unique parameter set for the blind calculations

As outlined above the DCH module in COCOSYS has been developed following the approaches in CONTAIN.

In COCOSYS only a single entrainment rate correlation is available representing a reference model for entrainment:

$$\varepsilon = 0.0025 K_c \left(1 + 360 \frac{\delta}{D_c} \right) \left(\frac{\rho_g v_g^2 \mu_d}{\sigma} \right),$$

with δ : film thickness, D_c : cavity diameter, ρ_g : gas density, v_g : gas velocity, μ_d : melt viscosity and σ : melt surface tension. Although in the analyses of lumped parameter codes the use of this correlation was suggested as not sufficient (see section C.1) this particular correlation was arbitrarily selected from the available ones in CONTAIN, as similar results can be obtained using different correlations with different coefficients.

A similar simplification was made for the modeling of particle trapping in COCOSYS: As the only reference model the gravitational fall model is provided in COCOSYS, since the consideration of particle trapping using this model is somewhat conservative.

In COCOSYS the chemical models allow simultaneous oxidation of metals by oxygen and steam. The mass and energy sources due to chemical reactions are considered in the coupled numerical solution of the mass and energy conservation equations in COCOSYS. The burning of hydrogen is simulated in COCOSYS with a simple recombination model.

For the blind calculations presented here a unique set of model parameters is used, which was obtained formerly from parametric post-test calculations for a range of other experiments, including the geometries of EPR (DISCO-H test series), French P'4 (DISCO-FH02) and the experiments at Surtsey (SUP-1 and SUP-2) [14]. For the fixing of the unknown parameters related with each of the most important processes these hypotheses have been used:

1. Video observations for the DISCO experiments show that the maximum containment pressure is observed at a time when there is still particle flow in the containment and that the pressure is reduced after the particles have been deposited on the structures. Based on this observation it is assumed that only the airborne particles contribute to the heating of the atmosphere and to chemical reactions whereas the settled particles had participated in a very efficient heat exchange process at the time of impact with the structure and effectively do not contribute to DCH any longer.
2. The slip factor, i.e. the ratio between gas and debris flow velocities, is considered as 1 (homogeneous flow), but calculations with slip factors $\neq 1$ are possible.
3. The airborne melt is homogeneously distributed in the different rooms.
4. The flow velocity v_g is computed by the total of gas volume fluxes exiting the cavity divided by a characteristic flow cross section (to be defined in the input).
5. Particle deposition is assumed to be governed by gravitational settling. For the subcompartment a virtually reduced zone height (~ 10 cm) is considered to account for the efficient trapping observed in experiments in which there is only a single exit from the cavity (leading to the subcompartment in that case). The reduced zone height for the subcompartment shall compensate for the requirement that particles have to take a 90° -turn in order to escape from the subcompartment to the containment. In that case the gravitational fall seems not the relevant deposition process in such rooms and will tend to underestimate the trapping rate in the subcompartment.
6. The particle size distribution is simplified by a monodisperse representation, for which the mean diameter was estimated by the Sauter diameter according to the experimental finding in DISCO-H04 (~ 0.47 mm). This distribution is static: At all times the particle distribution is characterized by this diameter, independent of actual gas velocities etc.
7. For the entrainment a Kutateladze cut-off number $K_{crit} = \frac{\rho_g v_g^2}{\sqrt{\sigma g (\rho_d - \rho_g)}} = 10$ is used as criterion for the onset of entrainment (limiting the process of entrainment only to sufficiently high gas velocities) in conjunction with a large cavity constant (10^4) for the entrainment rate. This leads to a very sharp, peak-like shape of the airborne amount of melt in the cavity as function of time i.e the entrainment is almost instantaneous at the time of gas blow through.
8. Regarding the heat transfer models the coefficients for radiative and convective heat transfer between airborne melt particles and atmosphere were reduced from 1.0 to 0.3, considering an effectiveness of the heat transfer mechanism of only 30 % compared to the theoretical values.

C.3.2. Blind calculations for P'4 geometry

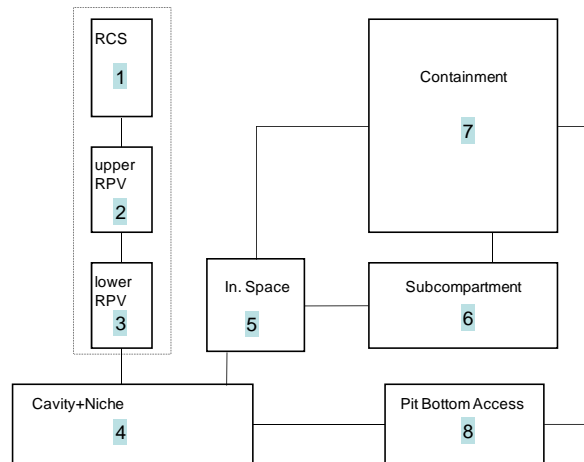


Fig. 25. Nodalization scheme in COCOSYS for the experiment DISCO-FH01

Two experiments in the DISCO facility for the French P'4 reactor were calculated in a blind condition: FH01 and FH03. The geometry of the experimental test section was subdivided into 8 cells as shown in Fig. 25. The experiment DISCO FH03 differs from FH01 with regard to the exit hole diameter (6 cm in FH03 instead of 3 cm in FH01) and the initial pressure (~ 2 MPa in FH03 instead of 1.6 MPa in FH01).

The cavity and the niche are combined into one single node, and the upper part of the cavity (= intermediate space) is separated from the lower part by a flow connection. This flow connection between the intermediate space and the lower part of the cavity is given by the cross section of the annulus.

Table 3: Comparison of blind COCOSYS-results with the experiments FH01 and FH03

quantity		FH01 (COCOSYS)		FH01 (experiment)		FH03 (COCOSYS)		FH03 (experiment)	
blowthrough time (s)		0.19		0.34		0.08		0.05	
end of blowdown (s)		0.78		1.50		0.31		0.38	
maximum containment pressure (M Pa)		0.37		0.31		0.55		0.56	
produced amount of FeO (mol)		12.6		-		13.8		-	
amount of hydrogen produced (mol)		13.6		40		15.4		44	
amount of hydrogen burned (mol)		15.7		28		47.8		83	
mass of debris (kg %) deposited in	cavity	4.31	40	4.91	46	2.95	27	4.59	45
	bottom access	2.55	23	2.63	25	2.97	27	1.74	17
	subcompartment	1.98	18	1.71	16	2.54	23	2.42	24
	containment	2.03	19	1.40	13	2.40	22	1.52	15

C.3.3. Blind calculations for Konvoi geometry

The blind calculation for the first Konvoi test KH01 was performed with the same set of model parameters as for the French P'4-design (FH01 and FH03). This should serve as a test for the portability of the models/model parameters to another plant design. Only the nodalization was adapted to the actual design of the Konvoi tests in the DISCO facility. The blind calculation for the second Konvoi test varied from the first test according to these particular details:

- The direct flow connection between upper cavity and subcompartment 2 was blocked in KH02 to account for a better agreement with the real plant design in that detail. This was done according to a change in the experimental set-up for KH02 in contrast to KH01.
- The oxidation models in COCOSYS were changed in the detail of the algorithmic sequence of oxidation reactions. In former results of the COCOSYS calculations there was always a substantial amount of FeO calculated which was formed by direct oxidation of metal with the oxygen of the atmosphere. This model did not take into account that there is indeed a coherent flow of melt and steam through the cavity and the subcompartment, which can not be modeled in a lumped parameter code using large-sized cells. Due to this coherent flow the oxidation of metal by steam is strongly preferred because of a better availability of steam in the vicinity of the airborne droplets. Therefore the algorithm for the oxidation reactions was changed so that the oxidation of metal by steam is generally preferred in the calculation.

Table 4: Comparison of blind COCOSYS-results with the experiments KH01 and KH03

quantity		KH01 (COCOSYS)		KH01 (experiment)		KH02 (COCOSYS)		KH02 (experiment)	
blowthrough time (s)		0.08		0.05		0.08		0.06	
end of blowdown (s)		0.35		0.45		0.43		0.42	
maximum containment pressure (M Pa)		0.45		0.42		0.41		0.50	
produced amount of FeO (mol)		7.1		-		7.0		-	
amount of hydrogen produced (mol)		3.7		37		7.5		33	
amount of hydrogen burned (mol)		47.3		53		29.9		69	
mass of debris (kg %) deposited in	cavity	3.44	32	1.41	14	4.51	42	4.56	48
	subcompartment1	4.53	42	4.26	44	5.52	51	4.60	48
	subcompartment 2	2.12	20	3.32	34	0.02	0	0.15	1
	containment	0.67	6	0.79	8	0.72	7	0.24	3

C.3.4. Conclusions from the blind COCOSYS calculations

The DCH module newly introduced in COCOSYS is strongly based on the DCH models of the U.S. code CONTAIN. This DCH-module in COCOSYS is being tested here with a fixed set of model parameters in blind calculations vs. four experiments performed in the DISCO facility for two different cavity designs: the French P'4 reactor and the German Konvoi reactor. The most important data to be compared with the experiments are summarized in Table 3 and Table 4.

The results of the blind calculations show that important physical quantities, e. g. the maximum containment pressure (Fig. 26) and the localized amount of debris dispersed in the rooms of the facility, are calculated by COCOSYS with good reliability using a unique parameter set for the relevant detailed models: For the distribution of melt the largest absolute error found for the local melt fractions among the four blind calculations performed is 18 %. For the predictions of maximum containment pressure a maximum relative error of 22 % was found.

However, the role of pre-existing hydrogen in the facility seems not sufficiently modeled. The model settings are currently based on the hypothesis that the maximum containment pressure is mostly related with the amount of debris dispersed from the cavity to larger rooms (subcompartment, containment) and not with the inventory of pre-existing hydrogen, since in former experiments this parameter was not sufficiently varied. For the P'4-experiments the calculations predict total melt fractions finally located in subcompartment and containment of about 37 % for FH01 and 45 % for FH03. From these data it has to be expected that the max-

models and the parameter set used the entrainment is calculated almost instantaneous and the local pressure peak in the cavity is strongly overestimated. This sharp pressure peak is referred to some weaknesses of the description of two-phase phenomena at the exit of the RPV.

D. CONCLUSION

The experimental database shows that the consequences of DCH are essentially related to cavity geometry, and to the pathways between it and other containment areas. In particular, it can be stated that the consequences of DCH are limited in reactors with no direct pathway between the cavity and the containment dome (closed pit). In contrast, the situation is less clear for reactors which do have a direct pathway between the cavity and the containment (open pit); the experiments showed that substantial fractions of corium may be dispersed into the containment in such cases, if the pressure in the reactor coolant system is elevated at the time of DCH. Combustion of the hydrogen produced by oxidation as well as the hydrogen initially present appears to be the crucial phenomenon for containment pressurization. It should be noted that DCH oxidation is difficult to extrapolate to reactor scenarios based on tests with simulant materials, which are much less reactive than corium components, especially zirconium. It is also difficult to extrapolate the effect of hydrogen combustion on the loads, because of uncertainty in the scaling of combustion rates under DCH conditions [26].

For the model development with view to the improvement of ASTEC a twofold strategy has turned out as result of the common analysis work of the SARNET group:

1. On the one hand side GRS uses and improves the lumped-parameter system code COCOSYS. The DCH models in COCOSYS allow in principle a more mechanistic modeling than currently the ASTEC-RUPUICUV model dedicated to DCH. A common parameter set has been proposed for the DCH models in COCOSYS which is tested in blind calculations for different reactor geometries. In these blind calculations the pressure increase in the containment relative to its initial pressure $\Delta P/P_0$ is predicted for different geometries (P'4, Konvoi) with an accuracy of 30 %. The local fraction of melt dispersed from the cavity is predicted with an absolute error of only ± 20 %. Besides these surprisingly good results some deficiencies have been identified: The burning of hydrogen – especially if pre-existing – and the transfer of released energy by hydrogen combustion seems not sufficiently modeled. The two-phase model for the flow of melt and steam from the RPV is too simplified with subsequent errors on the dynamics of melt entrainment and the pressure peak in the reactor cavity. Due to the complexity of the process and the poor spatial resolution of lumped parameter codes the parameters needed for entrainment rate correlations are very empirical. Improved approaches may be suggested on the basis of the studies with computational multi-fluid dynamics (CMFD) codes like MC3D.
2. On the other hand side MC3D is used by IRSN to study more mechanistic approaches for the melt dispersal phenomenon. With the use of MC3D with relatively coarse meshes a method of developing a dispersion correlation is elaborated. For different geometries (EPR, large pit reactors) the calculation results can be used to calibrate precisely such correlative approaches, as it has been shown for the case of the French P'4 reactors. For a full evaluation of the phenomenon a model of combustion is required. However, even codes dedicated to combustion have severe difficulties to evaluate this phenomenon with all its complexity. For MC3D it is envisaged to seek for a simplified combustion model. With the help of MC3D some deepened insights for the dispersion of the melt are found: It has been concluded, that 2D calculations may be a good approach for the 3D phenomenology. Also

the range of physical conditions for which the dispersion can occur can now be identified with good confidence. Based on this a range of conditions may be proposed for which the phenomenon cannot threaten the integrity of the containment. Further, with MC3D it is possible to consider some supplementary conditions that are usually not taken into account as e.g. the presence of water.

ACKNOWLEDGEMENT

Development and validation of COCOSYS are funded by the Federal Government of Germany (Ministry of Economics and Technology BMWi).

REFERENCES

- [1] Nuclear Engineering. Design, 164, Topical Issue on DCH, (1996)
- [2] M.M. Pilch, M.D. Allen, D.C. Williams, “Heat Transfer During Direct Containment Heating“, in Advances in Heat Transfer, G.A. Greene Ed., Academic Press, Vol. 29 (1997)
- [3] L. Meyer, M. Gargallo, “Low Pressure Corium Dispersion Experiments with Simulant Fluids in a Scaled Annular Cavity”, Nuclear Technology, Vol. 141, pp. 257-274, (2003)
- [4] L. Meyer, M. Gargallo, et al. “Low pressure corium dispersion experiments in the DISCO test facility with cold simulant fluids”, Report FZKA 6591, Forschungszentrum Karlsruhe (2006)
- [5] R. Meignen, D. Plassart, C. Caroli, L. Meyer, D. Wilhelm, “Direct Containment Heating at Low Primary Pressure: Experimental Investigation and Multi-dimensional Modeling”, NURETH-11, Avignon, France, (2005)
- [6] L. Meyer, G. Albrecht, et al., “Melt Dispersion and Direct Containment Heating (DCH) experiments in the DISCO-H Test Facility”, Report FZKA 6988, (2004)
- [7] L. Meyer, G. Albrecht, M. Kirstahler, “Corium Dispersion and Direct Containment Heating Experiments at Low System Pressure”, NURETH-10, Seoul, Korea, October 5-9 (2003)
- [8] L. Meyer, G. Albrecht, D. Wilhelm, “Direct Containment Heating Investigations for European Pressurized Water Reactors”, NUTHOS-6, Nara, Japan, October 4-8 (2004)
- [9] L. Meyer, I. Ivanov, S. Kisyoski, G. Albrecht, D. Popov, “Direct Containment Heating (DCH) in VVER 1000 Reactors, Physical Modeling and Experimental Results”, ENERGY FORUM 2006, Varna, Bulgaria, (2006)
- [10] L. Meyer, G. Albrecht, “Direct Containment Heating Experiments for Konvoi Power Plants”, ICAPP '08, USA, June 8-12, (2008)
- [11] L. Meyer, G. Albrecht, M. Kirstahler, M. Schwall, E. Wachter, “Separate Effects Tests on Hydrogen Combustion during Direct Containment Heating Events”, Report FZKA 7379, Forschungszentrum Karlsruhe, (2008)
- [12] L. Meyer, A. Kotchourko, “Separate Effects Tests on Hydrogen Combustion during Direct Containment Heating Events in European Reactors”, SMiRT 19, Toronto, Canada, August 12-17, (2007)
- [13] D. Wilhelm, “Recalculation of Corium Dispersion Experiments at Low System Pressure,” NURETH-10, Seoul, Korea, October 5-9 (2003)

- [14] T. K. Blanchat, M.M. Pilch, R.Y. Lee, L. Meyer, and M. Petit, "Direct Containment Heating Experiments at Low Reactor Coolant System Pressure in the Surtsey Test Facility," NUREG/CR-5746, SAND99-1634, Sandia National Laboratories, Albuquerque, N.M., (1999)
- [15] M. M. Pilch, A two-cell equilibrium model for predicting direct containment heating, Nuclear Engineering and Design, 164, pp. 61-94 (1996)
- [16] K. K. Murata, D. C. Williams, J. Tills et al., "Code Manual for CONTAIN 2.0: A Computer Code for Nuclear Reactor Containment Analysis", NUREG/CR-6533, SAND97-1735, (1997)
- [17] R. O. Gauntt, R. K. Cole, C. M. Erickson, R. G. Gido, R. D. Gasser, S. B. Rodriguez, M. F. Young, "MELCOR Computer Code Manual", Vol. 1: Primer and Users' Guide, Vol. 2: Reference Manuals, Version 1.8.5 May 2000, Sandia National Laboratories, USA, Albuquerque, SAND2000-2417/1+2, (2000)
- [18] R. E. Henry, C. Y. Paik, M. G. Plys, "MAAP4 - Modular Accident Analysis Program for LWR Power Plants", Fauske & Associates Inc., Prepared for Electric Power Research Institute, (1994)
- [19] H.-J. Allelein, S. Arndt, W. Klein-Heßling, S. Schwarz, C. Spengler and G. Weber, "COCOSYS: Status of Development and Validation of the German Containment Code System", Nuclear Engineering and Design, Volume 238, Issue 4, April 2008, Pages 872-889, (2008)
- [20] H. -J. Allelein, K. Neu, J. P. Van Dorsselaere, K. Müller, P. Kostka, M. Barnak, P. Matejovic, A. Bujan and J. Slaby: European Validation of the Integral Code ASTEC (EVITA), Nuclear Engineering and Design, Volume 221, Issues 1-3, April 2003, Pages 95-118, (2003)
- [21] W. R. Bohl and D. Wilhelm, "The Advanced Fluid Dynamics Model Program: Scope and Accomplishment", Nuclear Technology, Vol. 99, pp. 309-317, (1992)
- [22] R. Meignen, "Status of the qualification program of the multiphase flow code MC3D", Proc. of ICAPP'05, paper 5081, Seoul Korea, May 15-19, (2005)
- [23] R. Meignen, S. Mikasser, C. Spengler, A. Bretault, "Syntheses of Analytical Activities for Direct Containment Heating", ERMSAR-2007, Forschungszentrum Karlsruhe (FZK), Germany, June (2007)
- [24] S. Mikasser, R. Meignen, " Computation and analysis of the Direct Containment Heating dispersion process with the multiphase flow software MC3D", Proceedings of ICAPP 2007, Nice, France, May 13-18, (2007)
- [25] M. Pilch, C.A. Erdman, "Use of breakup time data and velocity history data to predict the maximum size of stable fragments for acceleration induced breakup of liquid drops", Int. J. of Multiphase Flow, Vol. 13, 6, 741 (1987)
- [26] D. Wilhelm, "The Challenge of Simplifying DCH Modeling," ERMSAR-2005, Aix-en-Provence, France, 14-16 November, (2005)